CHEMISTRY
A EUROPEAN JOURNAL

DOI: 10.1002/chem.200600893

Femtosecond Transient Absorption and Nanosecond Time-Resolved Resonance Raman Study of the Solvent-Dependent Photo-Deprotection Reaction of Benzoin Diethyl Phosphate

Chensheng Ma, Yong Du, Wai Ming Kwok, and David Lee Phillips*[a]

Abstract: A combined femtosecond transient absorption (fs-TA) and nanosecond time-resolved resonance Raman (ns-TR^3) study was performed to directly detect the dynamics and elucidate the mechanism of the excited state deactivation and solvent-dependent photo-deprotection pathways for benzoin diethyl phosphate (BDP) in neat acetonitrile (MeCN) and 75% H_2O/25% MeCN. Comparison of the TA spectral evolution observed in the two solvents provides explicit evidence that the photophysical deactivation of the BDP singlet excited state has little solvent dependence. The TA spectra also indicate the related internal conversion (IC) and intersystem crossing (ISC) processes occur rapidly on hundreds of femtoseconds and ~2–3 ps time scales, respectively. From this and in conjunction with a photochemistry study and ground state resonance Raman (RR) measurements, the TA results reveal that the phenacyl localized BDP triplet state (that is mainly $n\pi^*$ nature) is the common and immediate precursor to the photo-deprotection reaction in both solvents. However, the triplet deprotection follows different pathways in neat MeCN versus the largely water containing solvent. The deprotection reaction in MeCN was determined to occur with a ~11 ns time constant and the reaction was found to be an unimolecular process leading to elimination of the diethyl phosphoric acid apparently concurrent with cyclization to yield the benzofuran product. In the water mixed solvent, the triplet reaction was observed to proceed with a ~15 ns time constant and the reaction leads to not only the deprotection–cyclization but also a heterolytic dissociation to release the diethyl phosphate anion through a branching and competing mechanism. The ns-TR^3 spectra combined with relevant DFT calculations have been used to characterize the dynamics, structure and vibrational frequencies to help identify the important intermediates as well as to explore the reaction pathway leading to formation of the solvolysis product in the largely water solvent. A consecutive mechanism has been revealed for the heterolysis–solvolysis reaction in the water mixed solvent. The present work provides direct and irrevocable evidence for the dynamics and mechanistic description of the overall photophysics and deprotection related photochemistry for BDP.

Keywords: Raman spectroscopy · solvent effects · time-resolved spectroscopy · transient absorption

Introduction

Photochemically removable protecting groups (PRPGs) have found increasing utility in many applications demanding temporally and spatially controlled release of reactive species in situ.[1–8] Examples include a variety of phototrigger compounds which have been developed for potential use in physiology experiments. Among the various protecting groups in the literature, some aromatic α-keto groups[1,3,9,10] such as *p*-hydroxyphenacyl (*p*HP) cages[11,12,13,14] have gained interest due to their potential use as phototriggers for the fast and efficient liberation of various biologically active stimulants. Benzoin and substituted benzoin esters are another important class of aromatic α-keto compounds that display attractive photo-deprotection properties such as a rapid liberation rate, a relatively high quantum yield for release of leaving group and the generation of a highly fluorescent but inert benzofuran by-product.[1,10,15,16–21] The practical features of these compounds have led to their extensive development as PRPGs for inorganic phosphates,[1,15a,b,20a] nucleotides,[15c,16] carboxylates,[17,18a,19] carbamates[20b,21] and alcohols,[20c] etc. These

[a] Dr. C. Ma, Y. Du, Dr. W. M. Kwok, Prof. Dr. D. L. Phillips
Department of Chemistry, The University of Hong Kong
Pokfulam Road, Hong Kong S.A.R. (PR China)
Fax: (+852) 2857-1586
E-mail: phillips@hkucc.hku.hk

Supporting information for this article is available on the WWW under http://www.chemeurj.org/ or from the author.

compounds have also been exploited for use in lithographic synthesis[20d] and as photoliable linkers.[18b]

The versatile applications and the biochemical and synthetic relevance of the benzoinyl PRPGs have attracted considerable interest in understanding the photo-deprotection mechanism(s) of these compounds.[1,15,17,18a,19,20a,21,22] Previous studies have shown the diversity and complexity of the reaction pathways leading to deprotection. The photoproduct composition and reaction efficiency have been found to depend on many factors. These factors include the position and type of substituent(s) on the benzyl ring, the nature of the leaving group and the character of the solvent environment. Photolysis of desyl compounds can yield a complicated mixture of coupling and addition products. Two typical reactions occurring in normal organic solvent and solvents with high ionizing ability, respectively, form the groundwork for the desyl or substituted desyl compounds being exploited as PRPGs or cages in phototrigger compounds. In organic solvents such as MeCN and benzene, the photo-liberation is accompanied by cyclization of the benzoinyl cage into the corresponding 2-phenylbenzofuran (PBF) product. The PBF conversion efficiency was found to be highest for the desyl esters with a *meta*-methoxy benzyl substitution but to be relatively modest for unsubstituted desyl compounds.[17,18a,19,20a,21] In (a largely) aqueous solution, the corresponding PBF yield decreases remarkably compared with that observed in MeCN; in addition to PBF, a second product (which is the primary product in largely aqueous solvents) has been observed and assigned to the solvolytic nucleophilic addition product of the corresponding benzoin (BZ) or substituted benzoin compound based on various product analysis methods.[15a,18a] This solvent-dependence implies the solvent plays a crucial role in deciding the excited state reactivity and in controlling the competition between the reaction channels for the formation of the various products observed in different solvent environments.

While the product identities and the reaction conditions appear to be well-established, the underlying kinetics and details of the reaction mechanism(s) leading to the deprotection and the PBF and BZ by-product formation as well as the associated solvent dependence have remained unclear for the benzoin and substituted benzoin esters. Substantially different views and various intermediates have been proposed in previous studies to interpret the experimentally observed solvent effects and the influence of the ring substitution and leaving group on the desyl deprotection photochemistry. For example, triplet mechanisms including i) homolytic cleavage followed by electron transfer[1,10] and ii) an apparently single-step transformation through a rate-limiting formation of a cyclized biradical intermediate[15a] were proposed for the deprotection–cyclization of unsubstituted benzoin esters. In addition, a heterolytic triplet cleavage of the keto α-C–O bond yielding the triplet cation was also suggested to be responsible for the deprotection and solvolysis observed for a benzoin caged phosphate in a largely water containing solvent.[15a] Furthermore, singlet mechanisms including i) direct heterolytic cleavage of the ketone α-C–O bond producing the benzylic α-ketocation as a key intermediate[20a] and ii) the involvement of a intramolecular exciplex followed by heterolytic cleavage giving a short-lived cationic intermediate[17] were also suggested for the deprotection–cyclization of a series of 3′,5′-dimethoxybenzoin esters (DMBEs). In addition, the formation of a biradical intermediate followed by acetoxy migration was proposed to result in both the cyclization and solvolysis products observed for the 3′,5′-bis(carboxymethoxy)benzoin acetate compound in a buffered aqueous solution.[18a] To evaluate the preceding proposed mechanisms and substantiate the pertinent reaction pathways, real time kinetic information as well as unambiguous identification of the reactive intermediate(s) are needed. To our knowledge, direct and explicit evidence of this kind has been scarce for the desyl PRPGs (such as benzoin[15a] and substituted benzoin esters). To help provide this required information, a comparative femtosecond time-resolved transient absorption (fs-TA) and nanosecond time-resolved resonance Raman (ns-TR^3) study on the benzoin diethyl phosphate (BDP) photo-deprotection reaction in MeCN versus. largely water mixed MeCN solvent is reported here.

BDP is a representative unsubstituted desyl caged compound exhibiting the characteristic solvent-dependent deprotection photochemistry of benzoin esters [see Eqs. (1) and (2)].

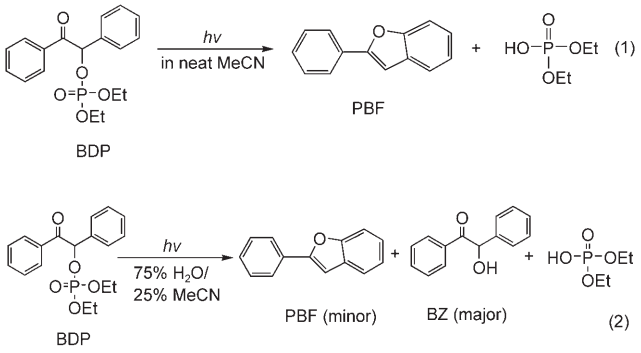

Givens and co-workers reported that photolysis of BDP in MeCN results in conversion to diethyl phosphoric acid and PBF with a nearly quantitative yield and a quantum efficiency of 0.28. The same product mixture and a similar quantum yield were also observed in MeOH and benzene.[1,10,15] However, in a largely aqueous solution, the deprotection reaction gives the solvolytic product BZ as the major product and the PBF as only a minor product.[15a] The predominant formation of the corresponding solvent nucleophilic addition product was also observed in highly ionizing solvents such as trifluoroethanol or hexafluoro-2-propanol.[15a] This product distribution and this typical solvent dependence make BDP very suitable example for a mechanistic study of the deprotection reactions of the desyl PRPG (or benzoin esters). Based on laser flash photolysis (LFP) and excited-state Stern–Volmer quenching studies, Givens

and co-workers provided convincing evidence for a triplet state mechanism and proposed two different pathways to be responsible for the solvent dependent product compositions.[15a] However, the predominant factor(s) controlling the mechanism and competition between the different pathways remains unclear and further direct kinetic and structural information are needed to explicitly identify the actual intermediates involved in the deprotection and elucidate the details of the reaction mechanism. Structural information on the related intermediates and their importance to the observed photochemistry also appears absent. The fs-TA and ns-TR^3 results presented here provide real-time monitoring of the reaction dynamics and direct spectral and structural characterization of the intermediates involved in the photochemistry. The ns-TR^3 spectra combined with density functional theoretical (DFT) calculations to determine the structures and vibrational frequencies provide solid evidence for the assignment of the reactive intermediates. To better understand the role of the solvent in influencing the reaction pathways, the effect of inter-solvent–solute hydrogen-bonding interaction and its structural relevance in the deprotection, cyclization and solvolysis reactions were also explored. These results shed new light on the photochemistry and lead to an improved understanding of the photo-deprotection mechanism for the desyl related PRPGs.

Results and Discussion

Steady-state photolysis

Figure 1 shows UV/Vis spectra obtained for the photolysis of BDP in MeCN solvent at varying irradiation times. It can be seen that, with an increase of the irradiation time, the BDP absorption spectrum (maxima at ~250 nm, spectrum a) in Figure 1) transforms gradually into an alternative spectrum with two absorption bands with maxima at ~300 and 230 nm (spectrum g) in Figure 1). The latter spectrum is identical to the absorption spectrum of PBF.[10,15a,20a,21] This together with the observation of the two well-defined isosbestic points at ~240 and ~265 nm clearly indicates a direct photo-induced conversion from BDP into PBF. The corresponding photochemistry measurements performed for BDP in 75% H_2O/25% MeCN solvent gave a similar spectral transformation but with the relative absorption ratio of the PBF product to the BDP reactant being substantially smaller than that observed in neat MeCN, which is consistent with the much reduced yield of PBF in the water mixed solvents relative to MeCN.[15a] Using the absorption extinction coefficient reported for PBF in methanol ($\varepsilon = 32220\,M^{-1}cm^{-1}$ at 302 nm)[10,15a] and assuming the same value in neat MeCN and the water mixed MeCN, the PBF quantum yield can be estimated to be roughly $\sim 0.35 \pm 0.1$ in neat MeCN and $\sim 0.19 \pm 0.1$ in the water mixed solvent. These values are comparable to those reported in literature.[1,10,15]

Since the absorption spectrum of the second expected product BZ in the water containing solvent closely resembles the BDP reactant (Figure S1 in the Supporting Information), it is expected that the UV/Vis spectral changes observed in the photolysis experiment does not afford a clear indication of the BZ generation. However, as illustrated below, the ns-TR^3 measurements do provide clear evidence for the dynamical formation of BZ in the same solvent. In general, the photochemistry observed here for BDP in the two solvents is consistent with previously reported results[15a,18a] and the photo-induced reactions depicted in Equatoins (1) and (2). More importantly, as demonstrated later in the fs-TA spectral evolution analysis, the broad and slightly structured ~300 nm PBF absorption band (with subpeaks at ~315 nm, ~300 nm, and 290 nm) can serve as a characteristic indication to track the cyclization dynamics leading to the PBF formation.

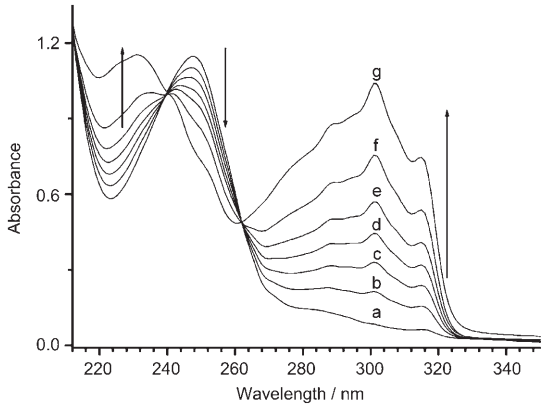

Figure 1. UV/Vis absorption spectra formed upon 267 nm laser photolysis of BDP in MeCN solvent, a) without, b) after 2 min, c) 4 min, d) 6 min, e) 8 min, f) 12 min, g) 60 min exposure to the laser light.

Resonance Raman (RR) spectroscopy

The RR spectra obtained with 267 nm excitation for BDP in neat MeCN and 75% H_2O/25% MeCN solvents and their respective comparison with the corresponding DFT calculated normal Raman spectra are displayed in Figure 2. The calculated spectrum for comparison with the MeCN spectrum is from the optimized geometry of free BDP molecule; while that for comparison with the mixed solvent spectrum is from the computation of the carbonyl hydrogen-bonded complex containing one water molecule. The optimized structures of the free and H-bonded BDP are displayed in Figure 3 and the corresponding geometric parameters are listed in Table S1 in the Supporting Information. Comparison of the experimental spectra obtained in the two solvents reveals essentially identical vibrational features with the same intensity distribution and frequencies except for the predominant carbonyl stretching mode showing a ~11 cm^{-1} frequency downshift upon going from the spectrum in MeCN (1708 cm^{-1}) to that in the mixed solvent (1697 cm^{-1}). The experimental observations and the frequency downshift of the carbonyl stretching vibration are well reproduced by the calculated results. A similar carbonyl stretching frequen-

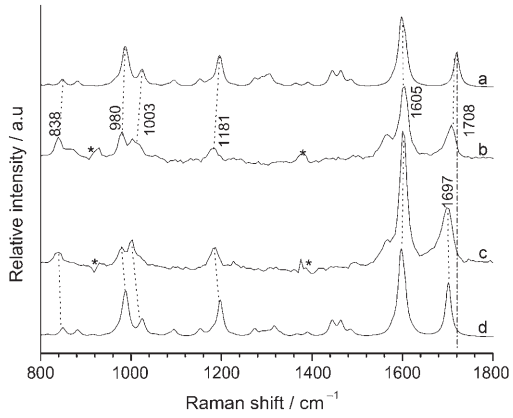

Figure 2. RR spectra of BDP in neat MeCN (b) and 75% H_2O/25% MeCN (c) and their respective comparison with the corresponding DFT calculated normal Raman spectra (a) and (d). The asterisks (*) mark solvent subtraction artifacts.

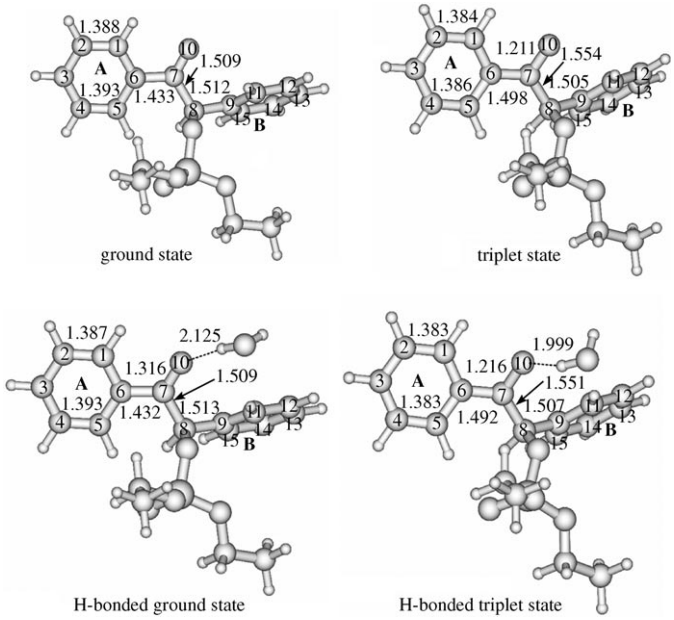

Figure 3. DFT optimized structures for the ground and triplet states of free BDP and the corresponding carbonyl H-bonded complexes.

cy was computed to shift down by ~18 cm^{-1} from the free BDP molecule to the H-bonded BDP molecule while the frequencies of all the other modes are nearly identical for both systems. The experimental and calculated frequencies and the corresponding normal mode descriptions for the observed RR vibrational features (refer to ref. [22] for a detailed list of the BDP vibrational analysis) are provided in Table S2 in the Supporting Information. It is therefore clear that the local inter-solute–solvent hydrogen-bonding interaction at the carbonyl site is responsible for the spectral difference observed in the two solvent systems. This is consistent with the localized nature of the H-bonding interaction and the slight structural differences found in the DFT calculations for the free and H-bonded BDP. The H-bonding leads to a slight increase in the carbonyl C–O bond length (~0.005 Å) and a modest variation in the relative reorientation between the benzoyl subgroup and benzylic moiety but with the other structural parameters kept nearly unchanged to those in the free BDP molecule. Based on the calculated total energies, the stabilization energy due to the H-bonding can be estimated to be ~5.4 kcal mol^{-1}. The calculations also find that, with a similar H-bonding strength, the carbonyl oxygen can H-bonded with an additional water molecule that locates at a position symmetric relative to the first one. This is consistent generally with the H-bonding configurations observed for other aromatic carbonyl compounds[23] and indicates that, different from the free BDP molecule in MeCN solvent, the ground state BDP molecule is present in the complex form with H-bonding to the surrounding water molecules in the largely water containing solvent.

In addition to the H-bonding effect, it is important to mention that, as summarized in Table S2 (Supporting Information), most vibrational features enhanced by the 267 nm excitation are due to the various normal modes associated with the phenacyl subgroup. This indicates that this subgroup is the chromophore responsible for the photoexcitation. This localized nature of the BDP photoexcitation is consistent with our previous excitation-dependent RR analysis.[22] From this as well as from knowledge of the nature of the transition of photo-excited aromatic carbonyl compounds,[11,19,22–26] it is obvious that the observed BDP RR spectra in the two solvents are both correlated with the strong $\pi\pi^*$ electronic transition (e.g. the S_3 state) of the phenacyl subgroup.

Fs-transient absorption (fs-TA) spectroscopy

Fs-TA measurement for BDP in MeCN: Figure 4 shows fs-TA spectra of BDP obtained in neat MeCN solvent with time delays up to 6000 ps after photo-excitation. To clearly display the spectral evolution in different time regimes, the spectra at early and late picosecond time-scales (corresponding to before and after 10 ps, respectively) are given separately in Figure 4. The temporal evolution of the early spectra (Figure 4a) shows a rapid conversion of the initial spectrum (the 0.6 ps spectrum) that absorbs strongly at 300 nm into a spectrum (the 10 ps spectrum) having a broad absorption with λ_{max} at ~350 nm. From Figure 4b, it can be seen that the ~350 nm spectrum decays gradually at later times and, at the expense of this decay, an additional spectrum with an absorption maxima at ~300 nm grows in. The observation of isosbestic points for both the early and late spectral conversions (at ~330 and 320 nm in Figure 4a and b, respectively) indicates there are direct dynamical conversions between two distinct state/species in each the case. The kinetics of these conversion processes can be followed by the time-dependence of the TA intensity at 350 and 310 nm, respectively. Such results are displayed in Figure 5 together with exponential fittings of the experimental data points. Obviously, the temporal change of the 350 nm band (Fig-

ure 4a) can be fitted by two exponentials with a ~2.3 ps time constant for the early-time growth and a ~11 ns time constant for the late-time decay. As seen in Figure 4b, the same corresponding time constants can also fit the early-time decay and late-time growth of the absorption at ~310 nm.

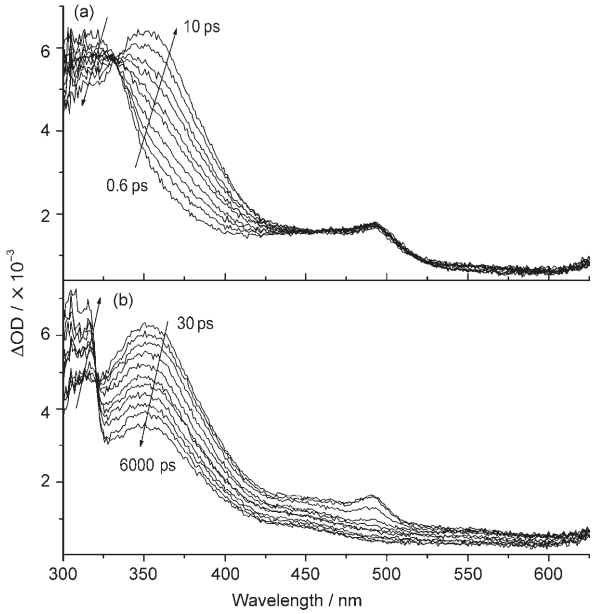

Figure 4. Fs-transient absorption spectra of BDP at a) early and b) later picosecond times recorded with 267 nm excitation in neat MeCN solvent.

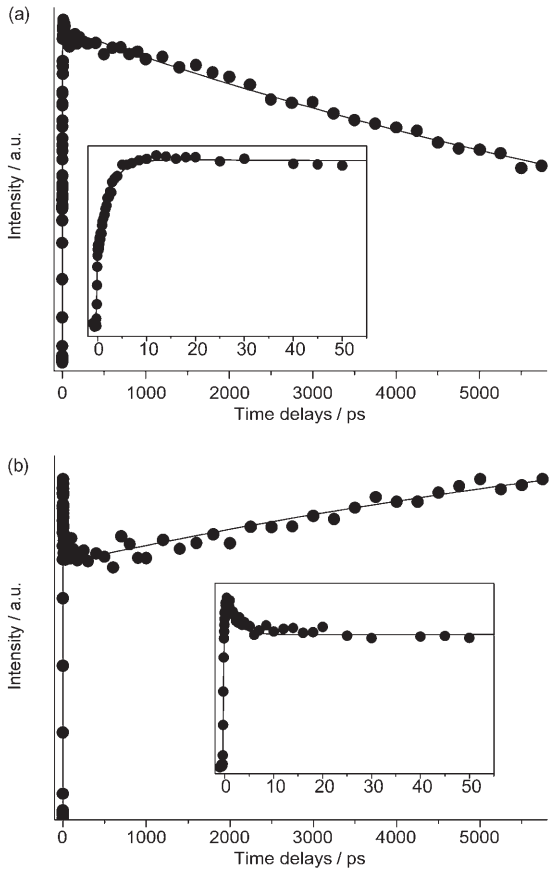

Figure 5. Time-dependence of the transient absorption spectra for BDP in neat MeCN at a) ~350 and b) ~310 nm. The solid lines indicate the kinetics fitting to the experimental data points using exponential functions. The inserts show the kinetics at early picosecond time delays.

The ~350 nm (λ_{max}) absorption spectrum (Figure 4, the spectrum observed at 10 to 50 ps) is clearly from the BDP triplet (T_1) state. Wirz and co-workers have reported the BDP triplet absorption spectrum within the 280–450 nm spectral region.[15a] The spectrum observed here is consistent with the reported spectrum but is displayed in a much broader spectral window. In addition, we note that the BDP triplet spectrum also closely resembles the triplet absorption spectrum of acetophenone[27,28] and the triplet absorption of the phenacyl group in phenacyl caged compounds.[3a] This indicates the triplet excitation is localized on the BDP phenacyl subgroup. From this assignment and the phenacyl localized nature of the triplet state, the observed ~2.3 ps time-constant spectral transformation (Figures 4 and 5) can be attributed confidently to intersystem crossing (ISC) conversion from the lowest singlet (S_1) state to the lowest triplet (T_1) state. The ~2.3 ps ISC time constant matches well the values of rapid ISC rate reported previously for a wide range of aromatic carbonyl compounds[11,22–29] and is consistent with the nearly unit triplet quantum yield reported for these compounds.[11,29,30] Therefore the initial spectrum (see the 0.6 ps spectrum in Figure 4a) can be assigned to the $S_1 \rightarrow S_n$ absorption from the BDP phenacyl S_1 ($n\pi^*$) state.[22]

The assignment of the S_1 singlet as the precursor state for ISC conversion is in agreement with a number of studies on acetophenone and other closely related compounds showing there is efficient ISC from the S_1 state into the triplet state.[22–24,26,28–40] The BDP S_1 absorption spectrum observed here has not been previously reported probably due to its short lifetime (~2.3 ps). An alternative assignment of the initial TA spectra to the 267 nm photo-populated S_3 state[11,19,22] and that the conversion occurs with the IC step being rate-determining (~2–3 ps) seems rather unlikely since previous relevant studies on the related aromatic carbonyl compounds have reported consistently a <100 fs lifetime for the S_3 state[11,23,32] and up to hundreds of femtosecond lifetime for the intervening S_2 state (weakly allowed $\pi\pi^*$ state).[32–35] This implies a rapid IC from the S_3 into S_1 state occurring with an upper-limit time constant of hundreds of femtoseconds. Considering the ~200 fs time-resolution of our TA setup, it appears reasonable to infer that IC process involved in the 267 nm excited BDP might be dominated by direct conversion from the S_3 into S_1 state that happens within tens to hundreds of femtosecond time scale,[11a] too fast to be easily detected by our present TA measurement. The S_1 spectrum is similar to the singlet absorption of the phenacyl subgroup of the *p*HP caged phototrigger compounds[11b] implying again the phenacyl localized excitation in the S_1 state. Consistent with the phenacyl localized absorption revealed by the RR spectrum, the observation of a

similar characteristic feature of the phenacyl associated singlet and triplet excited state spectra and the correlated ISC rate indicates the predominance of the phenacyl subgroup being responsible for the photo-excitation and early photophysical processes.

The late-time picosecond spectrum with the predominant absorption at ~300 nm (see Figure 4b) displays the characteristic structured UV absorption of the PBF cyclization product (see Figure 1). As displayed in Figure S2 (Supporting Information), this is shown by a direct comparison between the ~300 nm transient absorption spectrum (with the absorption due to the BDP triplet state subtracted) with the PBF UV spectra (spectrum g in Figure 1). Therefore the observed ~11 ns spectral conversion (Figures 4b and 5b) reflects a direct BDP triplet state reaction leading to the PBF production. This rather fast and straightforward BDP triplet to PBF cyclization is a remarkable reaction since it requires not only the net elimination of the phosphate leaving group and the 2′-benzylic proton but also a coupled spin flip. It is therefore necessary to be cautious about the identity of our late picosecond ~300 nm transient spectrum. In this context, we note that the spectrum is consistent with the ~300 nm ns LFP spectra (at 30 ns time delay) reported for BDP in MeCN by Givens and co-workers.[15a] In their work, the ~300 nm absorption has been assigned specifically to the PBF photoproduct based on a dynamic measurement for both the BDP absorption and emission spectra. This together with the close resemblance in the absorption spectral profile makes it quite certain for the tentative assignment of our late ~300 nm spectrum to the ground state of PBF. An alternative assignment of this absorption to other intermediates that may possibly occur in the triplet cyclization pathway appears implausible. Such transient species include the triplet state of BDP, the radical **1** and cation **2** intermediates possibly formed as

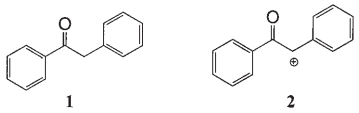

1 **2**

a result of the homolysis and heterolysis, respectively, of the keto α-C–O bond.[15,17–21] DFT computation at the random-phase approximation (RPA) with the B3LYP method and 6-311G** basis set found that the triplet state BDP has its strongest absorption at ~437 nm (with an oscillation strength f of ~0.6) and a modest absorption at ~338 nm (with f of ~0.2) (the details of the calculated RPA results are listed in Table S3 in the Supporting Information). Obviously, these absorption positions are not in accordance with the ~300 nm absorption observed here in the TA spectra and this implies the BDP triplet does not account for the experimental spectrum. For radical **1**, from the lack of the decarboxylation for the acyloxy radical, previous studies on benzoin and a series of methoxy substituted benzoin esters have suggested only a possible minor importance of the homolysis in the deprotection pathway.[17–20] As for cation **2**, our following result and discussion indicates evidently that it is featured by a ~570 nm absorption, rather than the ~300 nm absorption in Figure 4b. It is thus clear that cation **2** proposed previously to be an essential intermediate for the BDP photocyclization reaction is not actually involved in the cyclization pathway but rather is present as a key intermediate responsible for the BDP deprotection–solvolysis process occurring exclusively in the largely water containing solvent.

Fs-TA measurements for BDP in 75% H_2O/25% MeCN solvent: Figures 6 and 7 show the fs-TA spectra and the corresponding kinetics observed for BDP in a 75% H_2O/25% MeCN solvent. Obviously, the spectral features and the correlated conversion dynamics observed in the early-time picosecond spectra (10 ps and before in Figure 6a and insets in Figure 7a and b) parallels those observed in neat MeCN solvent. This indicates that the temporal evolution of the corresponding TA spectrum reflects the very similar ISC conversion (with a ~2.7 ps time constant as obtained by an exponential fit shown in the inserts in Figure 7) from the $S_1(n\pi^*)$ singlet state (represented by the 0.35 ps spectrum in Figure 6a) to the T_1 triplet (represented by 10–30 ps spectra in Figure 6a and b) excited state. Considering the remarkable differences in polarity and H-bonding ability between MeCN and water, the spectral and dynamic resemblance in the photophysics observed in the two solvent systems suggests there is only a modest influence of solvent property on these processes. This is consistent with the nearly solvent-independent ISC dynamics reported recently in our combined fs-time-resolved fluorescence (fs-TRF) and ps-TR^3 study on *p*HP caged phototriggers.[11]

However, the late time spectral evolution recorded in the largely water containing solvent displays distinctly different features from that observed in MeCN (Figure 4b and 5b). It

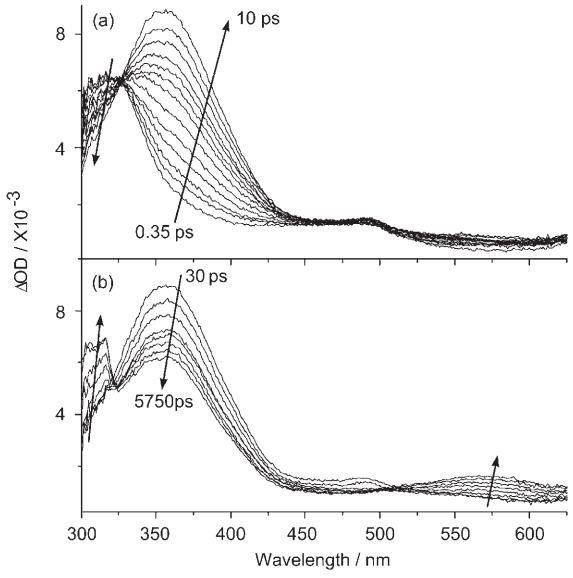

Figure 6. Fs-transient absorption spectra of BDP at a) early and b) later picosecond times recorded with 267 nm excitation in 75% H_2O/25% MeCN.

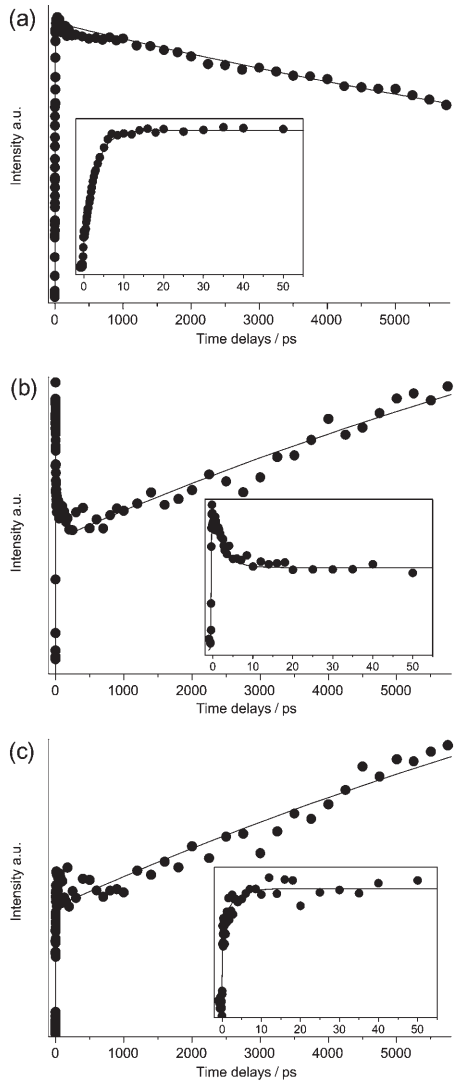

Figure 7. Time-dependence of transient absorption spectra for BDP in 75% H_2O/25% MeCN at a) 370, b) 305 and c) 570 nm. The solid lines indicate the kinetics fitting to the experimental data points using exponential functions. The inserts show the kinetics at early picosecond time delays.

can be seen from Figure 6 b that, as the BDP triplet spectrum decays, there are the simultaneously development of two absorption bands. Besides the common ~300 nm absorption band also observed in neat MeCN, an additional band with a broad absorption and a λ_{max} at ~570 nm is seen exclusively in this largely water containing solvent. The growth of the two latter bands are accompanied by isosbestic points at ~320 and 510 nm, respectively. The kinetics of the triplet decay and the development of the two new bands are followed by temporal variations in the TA intensity at typical wavelengths of ~370 (Figure 7a), 305 (Figure 7b) and 570 nm (Figure 7c), respectively. Exponential fitting of these series of experimental data points results in a ~15 ns conversion time from the triplet spectrum into the ~300 and ~570 nm absorption bands. The analogy of the ~300 nm band seen in the water mixed solvent to that in neat MeCN suggests that this band results from a species with the same identity, that is, the PBF product. Obviously, the ~570 nm band is from an alternative species, neither the BDP triplet state nor the PBF product. This band correlates well with the ~570 nm absorption band reported in a BDP nanosecond LFP spectrum (in aqueous solution with 4% MeCN) by Givens and co-workers.[15a] Based on DFT energy calculations, Givens and co-workers have associated this band with the triplet cation resulted from direct BDP triplet heterolytic cleavage of the phosphate leaving group.[15a] To confirm further this assignment and to track the associated reaction pathway so as to unveil its relevance to the solvolytic BZ product, ns-TR^3 experiments combined with DFT results for this intermediate are presented in the next section.

We note that the ~11 and ~15 ns BDP triplet decay times determined here in neat MeCN and H_2O/MeCN, respectively, are very close to the 10–25 ns triplet lifetimes reported by Givens and co-workers based on the indirect diffusion controlled triplet quenching study in these two kinds of solvents.[15a] The fs-TA results presented here provide, however, additional and unequivocal evidence to indicate that the triplet is i) the reactive precursor to the deprotection–cyclization reaction in MeCN and ii) the common precursor to the deprotection–cyclization and heterolytic deprotection leading to photosolvolysis (below) in the largely water containing solution. In the case of the largely water containing solvent, it is unlikely that the observed later time 300 nm band is from the same transient species responsible for the ~570 nm band even though both bands display similar developing dynamics (Figure 5b, 6b and c). This is because the species responsible for the ~570 nm band was found to lead eventually and solely to the solvolytic BZ product (see next section for details). This in turn leads to the product distribution shown in Equation (2). In addition, the photochemical results requires the ~300 nm band being assigned to the PBF product.

Ns-Time-resolved resonance Raman (ns-TR^3) spectroscopy and comparison with DFT calculation results

Ns-TR^3 study with a 532 nm probe wavelength: According to the fs-TA spectrum recorded in H_2O/MeCN (Figure 6b), a 532 nm probe wavelength was selected for the ns-TR^3 experiments to detect the intermediate responsible for the ~570 nm transient absorption band. Figure 8 displays representative ns-TR^3 spectra of BDP in 75% H_2O/25% MeCN acquired with time delays between the pump and probe pulses varying from 0 to 5000 ns. The temporal evolution of the spectra reveals a dynamic transformation from an early species (manifested by the 10 ns spectrum in Figure 8) into a late one (represented by the 200 ns spectrum in Figure 8) that decays on the microsecond time scale. By fitting a typical Raman band area with a Lorentzian function, Figure 9 displays the intensity time-dependence of the early species (represented by the 1560 cm^{-1} band area) and the later species (represented by the 1626 cm^{-1} band area). The kinetics shown in Figure 9 can be fit well by exponential decay and

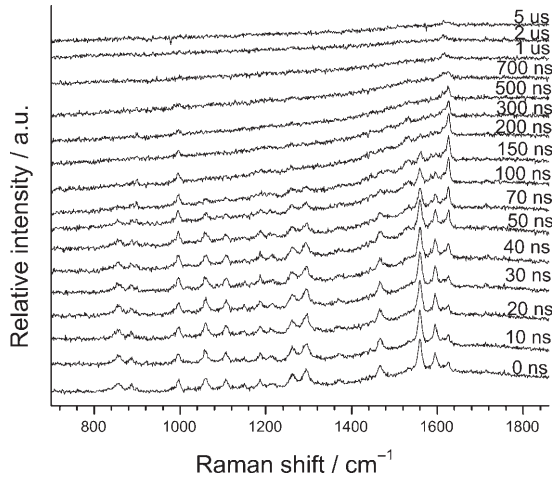

Figure 8. ns-TR^3 spectra of BDP in 75% H_2O/25% MeCN obtained with 267 nm excitation and a 532 nm probe wavelength at various time delays.

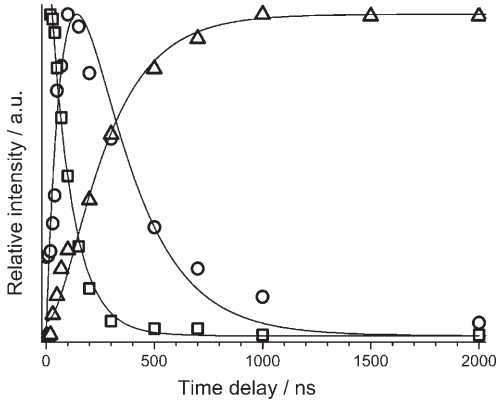

Figure 9. Time-dependence of the early (□) and the later species (○) for BDP in 75% H_2O/25% MeCN observed in the ns-TR^3 spectra displayed in Figure 8, and the kinetics for formation of the BZ product (△) as observed in the ns-TR^3 spectra displayed in Figure 12. The solid lines indicate the kinetics fitting based on Equations (3) and (4) in the text.

growth components as displayed by the solid lines in the figure. From the exponential fitting, a time constant of 102 ± 6 ns was estimated for decay of the early intermediate and a growth component with a similar time constant combined with a ~230 ns decay time was found for the late one. Further ns-TR^3 measurements reveal that the lifetime of the early intermediate becomes longer upon a nitrogen purge of the sample system (the corresponding ns-TR^3 spectra are given in Figure S3 in the Supporting Information). Under an oxygen purge of the sample, the early time species lifetime becomes shorter. In contrast, the lifetime of the late species is hardly affected by nitrogen or oxygen purging. The sensitivity of the early species lifetime to the oxygen concentration suggests a triplet nature for this species while the insensitivity observed for the later species implies it probably has a singlet character.

The benzoin triplet and singlet cation produced by heterolytic cleavage of the C–O bond connecting the phosphate leaving group and the desyl cage are the most plausible intermediates for the early and late species, respectively, observed in the ns-TR^3 spectra (Figure 7).[15a,17,20a,21] To investigate this probable assignment, (U)B3LYP/6-311G** based DFT calculations were done for the triplet and singlet cations. These calculations located more than one minima for both the triplet and singlet cations and found that the lowest energy of the singlet conformation is ~22.1 kcal mol^{-1}e more stable than the lowest triplet counterpart, in agreement with the singlet state as being the ground state of this cation species.[15a]

The calculations for the triplet cation located two minima with the carbonyl lying in the benzylic ring plane but being s-*cis* and s-*trans*, respectively, to the ring moiety. The s-*cis* conformation was calculated to be ~4.7 kcal mol^{-1} (including ZPE) lower in energy than the s-*trans* one. This together with the reported relatively large rotation barrier for conversion of the s-*cis* to s-*trans*-conformation[15a] suggests that the s-*cis* isomer would be predominantly responsible for the early time species seen in the ns-TR^3 spectra. The major structural parameters of the optimized s-*cis* triplet cation are listed in Table S4 in the Supporting Information and the structure is shown in Figure 10. Figure 11 displays a comparison and tentative correlation of the 10 ns TR^3 spectrum to the calculated Raman spectrum given by the s-*cis* triplet cation. It can be seen that the computed spectrum reproduces reasonably well the experimental spectrum. This helps to confirm its assignment to the triplet cation. Provisional vibrational assignments to the observed Raman features based on a direct comparison between the two spectra are listed in Table S5 in the Supporting Information.

In relation to the BDP ground state conformation (see Figure 3 and the structural parameters in Table S1 in the Supporting Information), the major structural difference displayed in the triplet cation is due to the conformation associated with the benzyl and carbonyl subgroups. For example, the benzyl C8–C9 bond and the bridging C7–C8 bond become significantly shorter (by ~0.09 and ~0.13 Å, respectively) suggesting that the two bonds gain noticeable double-bond nature in the triplet cation. This is also consistent with the lengthening (by ~0.03 Å) and shortening (by ~0.02 Å), respectively, of the benzyl ring shoulder and center C–C bond lengths. The benzylic ring of the triplet cation gains some quinoidal character in comparison to its ground state counterpart. The carbonyl bond becomes slightly longer by ~0.05 Å in the triplet cation and changes its orientation from being coplanar with the adjacent ring in the ground state to coplanar with the benzyl moiety in the triplet cation. This structural variation in the triplet cation suggests there is an increased extent of the benzyl conjugation in the triplet cation relative to the BDP ground state. In other words, the delocalization of the π electrons occur at the benzyl ring moiety in the ground state but extends to additionally involves the connecting C7–C8 and C8–C9 bonds as well as the carbonyl group in the triplet cation. The structure of the triplet cation and its differences from the BDP ground state are consistent with the frequency changes of

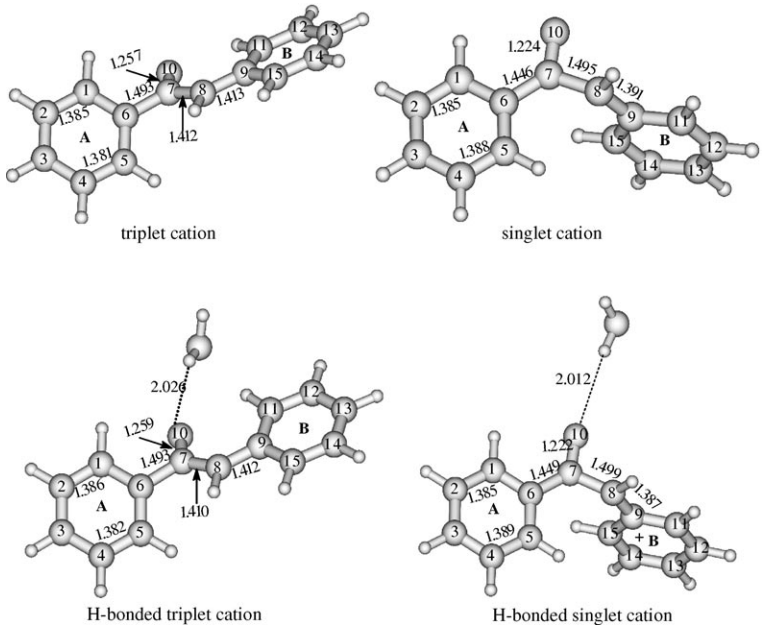

Figure 10. DFT optimized structures for the free triplet and the singlet cation and their respective carbonyl H-bonded complexes.

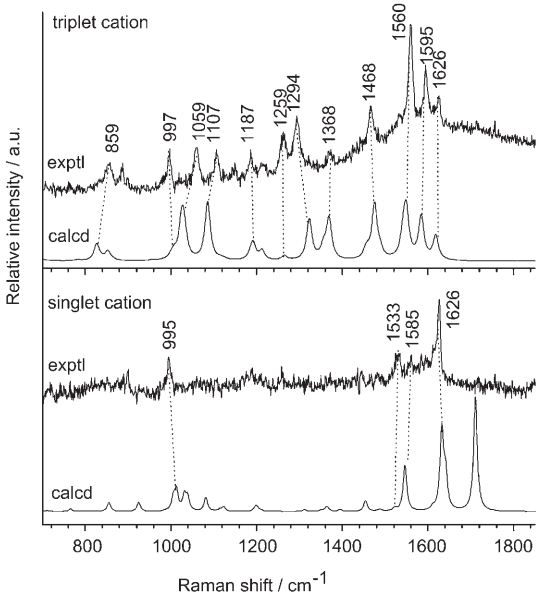

Figure 11. Comparison of the experimental and DFT calculated Raman spectra for the singlet and triplet cation. See the text for details.

the relevant vibrational modes observed in the two species. For instance, in agreement with the increased quinoidal character, the ring center C–C stretching of the benzylic ring displays a ~31 cm^{-1} frequency up-shift on going from the ground state (1595 cm^{-1})[22] to triplet cation (1626 cm^{-1}). In accordance to the noticeable shortening of the C7–C8 bond length, the vibrational feature contributed mainly by the stretching of this bond shifts up by ~158 cm^{-1} in the triplet cation (1186 cm^{-1}) relative to the ground state (1028 cm^{-1}).[22] However, there is no specific vibrational feature with a predominant carbonyl stretching motion in the triplet cation. According to the calculations, this is due to mixing of the carbonyl stretching motion with the benzylic ring carbon–carbon stretching vibrations. We note that most features observed in the ns-TR^3 spectra are due to vibrational motions associated with the benzylic ring and the nearby C-C chain (see Table S3, Supporting Information). This suggests that the extensively conjugated benzyl moiety included subgroups are the major chromophore probed by the 532 nm ns-TR^3 measurements and mainly account for the ~570 nm absorption band seen in the fs-TA spectrum (Figure 6b).

Calculations for the singlet cation located three minima with energy differences within ~0.002 kcal mol^{-1}. These minima have generally similar structures that differ mainly by modest variations in the carbonyl connecting C6–C7 and C7–C8 bond lengths (varying by ~0.04 Å). The three isomers exhibit almost identical structural parameters for the carbonyl connecting ring and the benzyl moiety; they all have the carbonyl group lying (nearly) at the connected ring plane and with a similar relative orientation of this plane with the benzyl plane. The isomers also give analogous calculated Raman spectra since the computed Raman features with noticeable intensities are predominantly the vibrational motions associated with the subgroups (mainly the two rings) with the common structural parameters. As a representative structure, the conformation of one such isomer is displayed in Figure 10 and the corresponding structural parameters are listed in Table S4 in the Supporting Information. A comparison between the corresponding computed Raman spectrum and a late-time ns-TR^3 spectrum (at 200 ns) is showed in Figure 11 together the spectra for the triplet cation. The calculated frequencies and tentative assignments of the experimental features made based on correlation of the experimental to the calculated spectrum are presented in Table S6 in the Supporting Information. It is obvious from Figure 11 that the experimental features seen in the ns-TR^3 spectrum are reproduced reasonably well by the calculations and this strongly supports assigning the spectrum to the singlet cation. The lack of the calculated carbonyl stretching feature at ~1700 cm^{-1} in the experimental spectrum is within expectations since the experimental spectrum was obtained with the resonance enhancement effect while the calculated one corresponds to a normal Raman spectrum. However,

considering the calculated result that the isomers have very close energy and give very similar Raman spectra, it appears that they may all contribute significantly to the experimental spectrum. This may also be a reflection that the singlet cation has a flexible structure in terms of the specific bond length for the bridging C–C bonds. It may be possible that a further search of the potential surface may locate additional minima with a generally similar geometry but slightly different bridging C–C bond lengths from those seen in the isomers already located. With the carbonyl group being far out of the benzylic ring plane and with the substantial single bond feature of the C7–C8 bond (Table S3, Supporting Information), the singlet cation has a lesser extent of the benzyl related conjugation than that of the triplet cation. This might account for the structural flexibility and could also be relevant to the subsequent reaction (see below).

Ns-TR^3 study on the formation dynamics for the photo-solvolysis product: To further explore the solvolysis reaction pathway and to determine the formation dynamics of the solvolytic product BZ, ns-TR^3 measurements with 267 nm pump and 267 nm probe wavelengths were done for BDP in 75% H_2O/25% MeCN. Figure 12 displays the acquired ns-TR^3 spectra recorded with the selected delay time up to ~2 μs. A RR spectrum from an authentic sample of BZ obtained under the same condition and by using 267 nm excitation is also shown in the Figure to compare with and to help identify the intermediate observed in the ns-TR^3 spectra. The temporal evolution of the spectra in Figure 12 shows the gradual growth of a series of features (mainly the strong feature at 1605 cm^{-1} and some weaker ones at ~1692 and ~1181 cm^{-1}) at the late nanosecond times. This reflects the formation of a new species in this time regime. Clearly, the newly developed spectrum closely resembles the RR spectrum of the authentic BZ, which indicates that the corresponding species can be attributed confidently to the BZ product. Thus, the temporal change of the transient BZ band area seen in the ns-TR^3 spectra represents directly the formation dynamics of the BZ product. The time-dependence of the Lorentzian fitted ~1605 cm^{-1} band area of the transient BZ is displayed in Figure 9 together with the kinetics obtained for the T^+ and S^+ species based on the ns-TR^3 measurements using the 532 nm probe wavelength. The general correlation of the kinetics obtained for the three species suggest a consecutive dynamics of $T^+ \xrightarrow{k_1} S^+ \xrightarrow{k_2} BZ$ with the k_1 and k_2 representing the rate constants for the cation ISC and the solvolytic addition step, respectively. In this reaction scheme, the temporal variation of the T^+ concentration [T^+] follows a single exponential decay with the time constant equal to the reciprocal of k_1, while the time-dependence of the S^+ and BZ concentrations ([S^+] and [BZ], respectively) are expressed, respectively, by Equations (3) and (4), where $[T^+]_o$ refers to the initial concentration of the T^+ precursor.

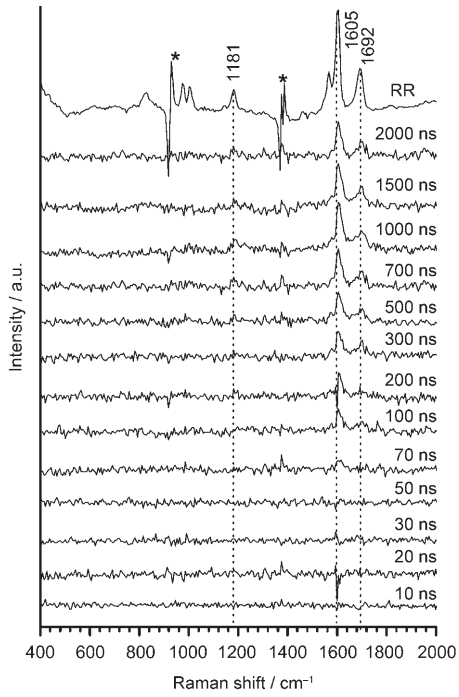

Figure 12. ns-TR^3 spectra of BDP in 75% H_2O/25% MeCN after 267 nm laser excitation and using a 267 nm probe wavelength with the time delays varying from 0 ns to 2000 ns. A resonance Raman spectrum of an authentic sample of BZ recorded with 267 nm excitation is displayed at the top.

$$[S^+] = [T^+]_0 \frac{k_1}{k_2 - k_1}[e^{-k_1 t} - e^{-k_2 t}] \quad (3)$$

$$[BZ] = \frac{[T^+]_0}{k_2 - k_1}[k_2(1 - e^{-k_1 t}) - k_1(1 - e^{-k_2 t})] \quad (4)$$

Provided that the ISC from T^+ to S^+ is the predominant channel to deactivate the T^+ population, the k_1 in Scheme 1 can be taken as the decay rate of T^+ determined by the 532 nm probed ns-TR^3 measurement ($k_1 = 1/\tau$ with $\tau =$ 102 ns). With this value for k_1 and based on Equations (3) and (4), the least squares simulation has been done to fit the kinetics result observed for the [S^+] and [BZ] concentrations. As displayed in Figure 9, this gives a reasonable fit to the experimental data and results in a rate of k_2 corresponding to a time constant of ~210 ns.

DFT calculations for the BDP triplet state and H-bonding configurations

Our fs-TA results (Figures 3 and 5) indicate clearly that the BDP triplet is the reactive precursor to the photo-deprotection reaction. It is therefore necessary to gain information about the structural and electronic properties of the BDP triplet. Our attempt to obtain a ns-TR^3 spectrum for the triplet state was hindered by overwhelming fluorescence from the PBF product. We have then performed open shell DFT calculations for this state and the computed energy and the optimized structural parameters for the triplet state are listed in Table S1 in the Supporting Information and the optimized triplet conformation is displayed in Figure 3.

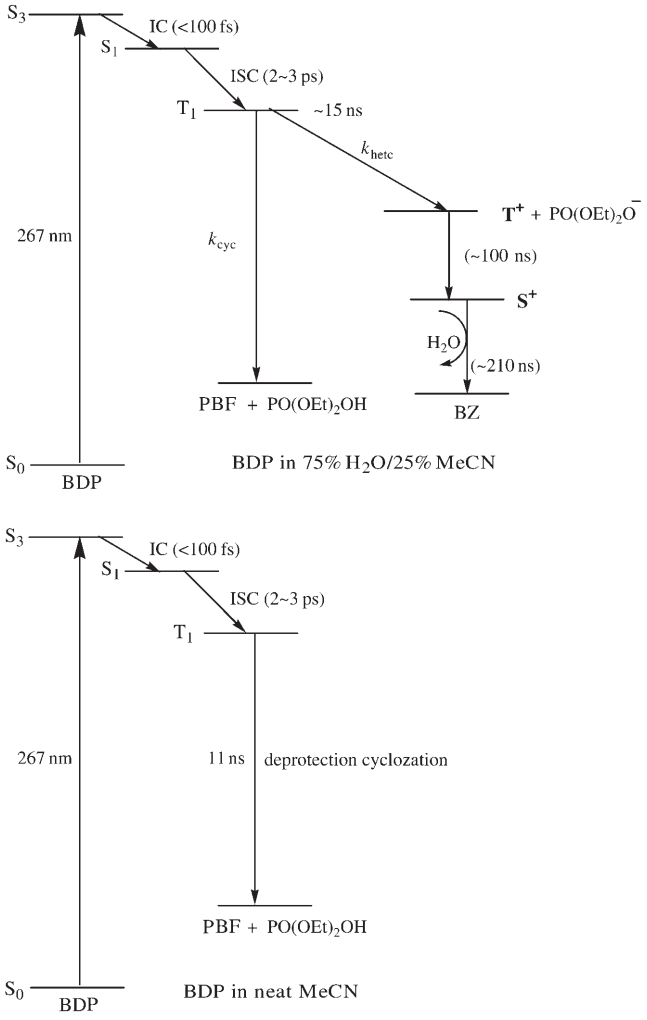

Scheme 1. Deactivation and deprotection reaction pathways of 267 nm excited BDP in neat MeCN and 75% H_2O/25% MeCN.

From the computed total energy (including ZPE) for the BDP triplet state and the ground state, a triplet state energy of ~64.4 kcal mol^{-1} can be estimated. This value is comparable to the ~73 kcal mol^{-1} triplet energy as given by a BDP phosphorescence spectrum.[1,10,15a,c] In terms of the structural changes in the triplet state, the triplet and singlet structures differ mainly by the conformation of the phenacyl subgroup. For example, upon going from the ground state to the triplet state, the carbonyl bond lengthened by ~0.1 Å and twists out of the phenayl plane by ~12°. The carbonyl connecting C6–C7 and C7–C8 bond shorten by ~0.07 and 0.05 Å, respectively, and the phenacyl ring gains a little quinoidal feature from slight increases and decreases of bond lengths for the ring shoulder C–C bonds and the center C–C bonds, respectively. On the other hand, the geometric parameters related to the benzyl group, the phosphate leaving group as well as the relative orientation of the benzylic ring with the carbonyl adjacent ring remain quite similar in the two states. This phenacyl localized structural variation in the BDP triplet state versus the ground state coincides and is consistent with the phenacyl localized excitation feature inferred above for the BDP triplet based on the fs-TA analysis. The calculated spin densities together with the triplet structure suggest a mainly nπ* nature triplet with an electron-deficient carbonyl oxygen. This is consistent with the triplet feature reported for unsubstituted phenyl alky ketones.[27,28,30,31]

To examine and evaluate the possible influence of the solvent–solute H-bonding associated solvent effect, we have done (in parallel with the BDP singlet ground state computations) DFT calculations considering the carbonyl H-bonded configurations for the BDP triplet (T_1) as well as the triplet cation (T^+) and the singlet cation (S^+) species. In general, these calculations suggest that the presence of the H-bonding interaction can lead to energy stabilization as well as modest structural modifications. The optimized structural parameters and the stabilization energies obtained for the H-bonded conformations are summarized in Tables S1 and S4 in the Supporting Information together with the corresponding results calculated for the free conformations. The structures for the DFT optimized H-bonded complexes are displayed in Figure 3 and 10 together with the free counterparts. It can be seen that, like the case of BDP ground state, whilst the H-bonding does not cause significant changes in the bond lengths, it does introduce noticeable variations in the relative orientations among the subgroups of the benzyl moiety, the carbonyl group and the carbonyl connected ring. This is particularly true for the BDP T_1 state and the S^+ species. From the calculated energy, the H-bonding stabilization energies are estimated to be ~4.8 kcal mol^{-1} for T_1 and 6.9 and 7.2 kcal mol^{-1} for the T^+ and S^+ species, respectively. The magnitudes of these energies are close to or even stronger than the corresponding BDP ground state (S_0) stabilization energy (5.4 kcal mol^{-1}). Since our RR experiment reveal that the BDP S_0 state is present in the complex form with the carbonyl H-bonding to surrounding two water molecules in 75% H_2O/25% MeCN. This implies that, in the same solution, the BDP T_1 state and the T^+ and S^+ species should also be in the corresponding H-bonded forms.

Summary of the photodeprotection pathways of BDP in MeCN and 75% H_2O/25% MeCN: Our fs-TA results obtained after the 267 nm photolysis of BDP in neat MeCN and in 75% H_2O/25% MeCN indicate that the BDP triplet is formed, barely dependent on solvent property, with a ~2–3 ps time constant by ISC from the S_1 excited state. A comparison of this ISC time with the dynamics determined for the photochemical reactions (represented initially by the ~10–15 ns triplet decay time constant, Figures 5 and 7) reveals that this state is the common precursor to the subsequent photochemical events in both of the two solvent systems. This is consistent with the corresponding results reported by Givens and co-workers.[15a] Corroborated with the phenacyl located singlet and triplet excitation as indicated by our RR and fs-TA results, the photophysics dynamics obtained here for the deactivation of the 267 nm excited S_3-(ππ*) state of BDP resembles closely to the rapid and solvent independent ISC from the S_1 to the lowest triplet state

observed generally for most aromatic carbonyl alkyl ketones in the solution phase.[11,23–29] This combined with the very efficient IC (with a time constant within hundreds of femtoseconds) from the S_3 and S_2 state ($\pi\pi^*$, formed due to ~250–300 nm excitation)[11,32–35] to the S_1 state ($n\pi^*$, formed due to >300 nm excitation) has been suggested to account for the high and substantially excitation wavelength independent triplet formation yield for these compounds.[29,30] Due to the BDP deprotection proceeding on the triplet manifold, the insensitivity of the triplet yield to the excitation wavelength suggests the deprotection efficiency to be also independent of the excitation wavelength. Indeed, as reported by Givens and co-workers, the desyl deprotection–cyclization reaction actually occurs with a similar efficiency over a broad range of excitation wavelength ranging from the deep UV to the far UV region.[15a] This indicates that the desyl photo-liberation does not necessarily require direct $S_1(n\pi^*)$ excitation, a condition that has been speculated to be essential for the desyl deprotection and cyclization.[17,18a,19,20a,21]

The phenacyl localized nature of the BDP triplet state combined with the triplet identity as the photoreaction precursor indicates that the BDP photo-deprotection is primarily the photochemistry of the phenacyl triplet state rather than the photodissociation chemistry associated with the singlet state of the benzylic subgroup[36–38] as proposed in some of the previous studies.[17,19,20a,21]

In neat MeCN, the decay of the triplet leads to an apparently single-step phosphoric acid elimination and cyclization reaction yielding the PBF product with ~11 ns time constant. Such a seemingly straightforward and efficient BDP triplet to PBF ground state transformation is an amazing reaction. For the reaction to occur, it requires extensive electronic reorganization and conformational rearrangement such as achieving an overall planar arrangement (as in the PBF product)[39] from the highly non-planar triplet conformation (see Figure 3 and Table S1, Supporting Information); it also needs an ISC at some point along the reaction pathway to bring the system from the triplet manifold to the singlet ground state. Considering the dependence of the deprotection–cyclization yield on the leaving group ability,[21] it is reasonable to infer that the reaction could create a charge in the transition state such that the departing leaving group may act as (to a certain extent) the hydrogen-abstracting base to facilitate the deprotonation of the 2′ carbon so as to assist the cyclization reaction. However, the small kinetics and yield dependence of the reaction to the change in the solvent polarity (from $\varepsilon=2.3$ for benzene to $\varepsilon=35.9$ for MeCN)[1,10,15] suggests that the transition state would be only modestly polarized during the liberation of diethyl phosphoric acid and the apparently concurrent cyclization process.

It is interesting to note at this point that the phenacyl located $n\pi^*$ nature triplet state of BDP is analogous to the triplet of phenacyl caged phenylacetate (PPA),[3a] *ortho*-methyl substituted phenacyl esters,[9] acetophenone and acetophenone derivatives[27,28] in terms of both the spectral features and the electronic character. This suggests they may also display similar triplet reactivity. For the latter compounds, either the intermolecular triplet carbonyl hydrogen abstraction (from the solvent) or the intramolecular carbonyl hydrogen abstraction pathway has been identified as the predominant initial photochemical step for the photochemistry. From this and the ~11 ns BDP triplet cyclization time constant, it may be conceivable that the BDP reaction could also originate from an intramolecular triplet carbonyl absorption of the benzylic 2′ hydrogen. Further theoretical calculations could be helpful to help determine the conformational details of the transition state and provide a more in depth molecule-level description to this intriguing reaction pathway.

In the largely water solvent, in addition to the deprotection–cyclization reaction, the triplet deactivation leads also to a heterolytic dissociation to liberate the phosphate leaving group in a competing and branching manner. The occurrence of the heterolytic cleavage is indicated by and confirmed by our combined ns-TR^3 (with a 532 nm probe wavelength) and DFT results that identify the triplet cation (T^+) as the initial heterolytic product. The temporal evolution of the ns-TR^3 spectra in conjunction with the DFT calculations also indicate that ISC of the T^+ species into the S^+ species with a ~102 ns time constant is followed by decay of the S^+ within the hundred nanoseconds time scale. Correlation of the S^+ decay kinetics with the formation kinetics of the solvolytic product BZ as observed by the 267 nm probe ns-TR^3 results indicates there is a sequential pathway for the solvolytic addition reaction.

An overall reaction scheme consistent with our previous result is displayed in Scheme 1 for the photodeprotection and solvolysis pathway of BDP in the two solvent systems.

According to this scheme, the triplet decay rate in the water mixed solvent is the sum of the reaction rate for the cyclization (k_{cyc}) and heterolysis (k_{het}). Therefore, the slightly slower triplet decay rate in the largely water solvent (~15 ns time constant) than that in neat MeCN (~11 ns time constant) implies a noticeably slower k_{cyc} in the former than later solvent. Considering the predominance of the solvolysis BZ product and assuming a ~25% of the chemical yield of PBF in the water mixed solvent, the k_{cyc} in the mixed solvent can be estimated roughly to be at least four times smaller in magnitude than that in MeCN.

The BDP ground state RR results together with the DFT results considering the carbonyl H-bonding interaction with the solvent water molecule(s) shows there is noticeable energy stabilization caused by the H-bonding. This suggests that, in the highly aqueous solution, not only the BDP ground state species, but also the other relevant intermediates involved in the excited state processes are present in the carbonyl H-bonded forms. At least as part of the first solvent shell, this H-bonding configuration may affect the triplet state reaction and contributes to the difference in the triplet deprotection dynamics and pathway observed in the largely aqueous solution versus neat MeCN where the H-bonding interaction is absent.

Heterolysis–solvolysis and deprotection–cyclization reactions in a largely water containing solvent

Extensive studies have shown that the kinetics and products of aromatic ketone photoreaction may be altered significantly in water compared with organic solvents.[11–13,15a,18a,23,40–44] This has been attributed generally to the solvent effect associated with the high polarity, high ionizing and high H-bonding ability of water. In the case of BDP, this solvent effect may mainly manifest itself as follows: i) by stabilization of the closely lying ππ* state and destabilization of the lowest nπ* state,[23,40–45] the high polarity and high H-bonding capacity of water could introduce increased ππ* character into the original nπ* dominated BDP triplet state. This in turn could lead to a decreased reactivity for the nπ* based reactions (the deprotection–cyclization). ii) As indicated by our DFT results on the carbonyl H-bonded complex, the incorporation of the H-bonding interaction can alter the triplet conformation especially in terms of the relative orientation among the two ring planes and the carbonyl group. This could result in a conformational effect and influence the triplet reaction. iii) The high ionizing ability combined with the high polarity of water provides a favorable environment to help drive and encourage heterolytic dissociation.[11,46–49]

The three factors could all contribute to varying degree to the different reaction pathways observed for BDP in the largely water containing solvent compared to in the neat MeCN solvent. However, the i) factor appears to be of minor importance since our fs-TA result show that, in either 75% H_2O/25% MeCN or in pure MeCN, the BDP triplet exhibits a similar absorption band with the λ_{max} at ~350 nm which is characteristic of an nπ* character triplet.[3,27,28] A typical ππ* character triplet state for aromatic ketones show an absorption with the λ_{max} at ~400 nm.[11b] The qualitatively similar nπ* triplet character in the two solvent systems is also supported by the fact that the BDP triplet deprotection–cyclization reaction also occurs to a significant extent in the largely water containing solvent. The slower k_{cyc} in the water mixed solvent than in the neat MeCN solvent may reflect the significant sensitivity of the deprotection–cyclization reaction to conformational factors. This appears fairy reasonable since this one-step reaction does necessitate a high degree of structural reorganization (see above section). Therefore, the H-bonding induced triplet geometric change combined with the bulky H-bonded triplet conformation (involving at least two H-bonded water molecules at the carbonyl site) may constitute a steric factor retarding the required structural rearrangement so as to increase the reaction barrier height leading to a decrease in k_{cyc}.

The additional opening of the heterolysis channel for BDP in the largely water containing solvent is obviously relevant to the solvent effect iii). Solvent-assisted intramolecular dissociative charge transfer from the phenacyl triplet π* orbital to the bond-breaking σ* orbital has been proposed to account for β-heterolysis of *p*HP caged phototriggers[11,12] and of radical anions of α-aryloxyacetophenones.[50,51] The BDP triplet heterolysis observed here may follow a similar mechanism where a significant degree of polar solvent reorientation is required to facilitate and accommodate the charge transfer so that the appropriate solvation of the triplet by the solvent ionizing and polarity ability becomes one of the most important factors in influencing the height of the relevant reaction barrier. Moreover, the stability of the heterolysis produced T^+ intermediate and the good nucleofugal property of the diethyl phosphate leaving group[52] are also of equal importance to jointly account for the occurrence of the efficient heterolytic deprotection in the largely water containing solvent. With a pK_a value of 1.4 for the conjugate acid,[11,48] the diethyl phosphate leaving group is a good nucleofuge; and photoheterolytic cleavage has been reported for many systems bearing the phosphate moiety as a leaving group.[11,47–49]

According to the DFT calculated structure and Mulliken charge distribution, the stablization of the incipient T^+ carbocation is due to the resonance conjugation with the adjacent π system. Thus, the positive charge formed in the heterolysis reaction is not localized at the benzylic carbon undergoing the ionization but is instead delocalized into the adjoining π-electron system. In largely polar environments such as a largely water containing solvent, the high stability of T^+ and the counterpart phosphate anion not only enable the heterolysis to compete with the deprotection–cyclization reaction but also facilitate the geminate ion pair separation so as to compete with the reverse ion recombination process. However, the conjugation-induced stabilization of T^+ may at the same time increase the "intrinsic barrier" for the T^+ to be trapped by the solvent for undergoing the solvolytic nucleophilic addition.[53,54] This may, on the other hand, constitute one of the important reasons for the observed stepwise BDP solvolysis scheme and a rationale for the necessary involvement of the S^+ species as the immediate nucleophilic addition precursor in the solvolysis pathway. Our calculations suggest a lesser extent of conjugation in S^+ than in T^+ and a substantial positive charge distribution on the S^+ benzylic carbon that makes this carbon well suited for solvent water nucleophillic attack leading to the formation of the BZ product.

For the branching mechanism of the BDP triplet deprotection–cyclization and heterolysis–solvolysis in the water mixed solvent, the relative yield of the PBF cyclization product and the BZ solvolysis product may reflect the relative efficiency of the two competing reaction channels. This relative yield of PBF and BZ would be expected to be governed by the relative barrier heights correlated with the respective reaction pathways. In this context, the predominance of the BZ product over PBF product observed in this solvent may imply there is a substantially lower triplet reaction barrier associated with the heterolysis–solvolysis reaction than with the deprotection–cyclization reaction. This is within expectations since the heterolysis reaction is generally associated with a highly polar transition state whereas the transition state correlated with the cyclization has been inferred to be modestly polar, which allows the high solvent

water polarity to favor the former reaction more than the latter one.

In general, the comparison of the excited state photophysical deactivation and photochemical reaction established here for UV photolysis of BDP in MeCN and H_2O/MeCN demonstrate the importance of the solvent environment in controlling the excited state reaction pathway. These results afford new examples of phenacyl triplet based β-elimination pathway and contribute new insight into the versatile deprotection chemistry of the phenacyl caged compounds. Further work on the photo-deprotection mechanism and its (probable) solvent dependence for DMBEs is planned in this lab to explore the remarkable substitution effects caused by the benzylic *meta*-methoxy substitution[17–21] and its correlation with the deprotection pathways revealed here for the non-substituted BDP.

Conclusion

We report here a combined fs-TA and ns-TR^3 spectroscopic study to detect the dynamics and mechanism of excited state deactivation and deprotection for BDP in neat MeCN and 75% H_2O/25% MeCN. The ns-TR^3 spectra in conjunction with DFT calculations have been used to characterize the structure and vibrational frequencies so as to help identify important intermediates involved in the excited state processes. DFT calculations based on a solvent–solute intermolecular H-bonded complex model have been adopted to explore the conformational changes induced by the H-bonding interaction and its relevance to the excited state reaction pathway in largely water containing solvents. Our study provides direct time-resolved evidence that the excited state photophysical deactivation due to the IC and ISC conversion occurs rapidly on the hundred of femtoseconds and several picosecond time scales, respectively. It has been revealed unequivocally that, independent of the solvent property, the phenacyl localized nπ* triplet is the common and immediate precursor for the photo-deprotection reaction. However, the triplet deprotection reaction has been found to follow different pathways in neat MeCN and in the largely water containing solvent. In MeCN, the triplet deprotection is an apparently a single-step process leading to the elimination of the diethyl phosphoric acid accompanied with cyclization to form a benzofuran product and the reaction has been found to occur with a ~11 ns time constant. In the largely water containing solvent, the triplet reaction has been determined to proceed with a ~15 ns time constant and in addition to the deprotection–cyclization, the reaction also results in a heterolytic dissociation leading to the liberation of the diethyl phosphate anion through a branching and competing mechanism. The heterolysis is demonstrated explicitly by direct observation and identification of the triplet cation as the initial product. The correlation of the dynamics and the structural characterization of the intermediates indicates that the triplet cation transforms subsequently into the corresponding singlet cation by ISC conversion with a ~100 ns time constant. The singlet cation then reacts further with the solvent water to yield the solvolytic nucleophilc addition product benzoin with a time constant of ~210 ns. The decrease of the cyclization rate in the water mixed solvent compared to the neat MeCN solvent is attributed mainly to a steric retarding effect associated with the carbonyl H-bonding configuration. It is suggested that three factors are important and jointly account for the occurrence of the heterolysis pathway in the largely water containing solvent: the high ionizing and polar ability of solvent to drive the heterolytic dissociation, the good nucleofugal property of the leaving group to make the bond breaking more feasible and the stability of the cation intermediate formed by the heterolytic dissociation to assist the heterolysis cleavage.

Experimental and Computational Section

Materials: BDP was synthesized following the method detailed in reference 10. The identity and purity of the BDP sample was confirmed using NMR, UV absorption, and mass spectrometric data. Spectroscopic grade MeCN and deionized water were used as solvents for samples used in the experiments.

Photochemistry experiments: The photochemistry of the photo-induced reaction for BDP in MeCN and H_2O/MeCN mixed solvent was monitored by measuring the UV/Vis absorption spectrum of the sample solution (~0.06 mM concentration) after exposure to an unfocused 267 nm laser line (~1 mJ) from the fourth harmonic of a nanosecond Nd/YAG Q-switch laser. The sample solution was put in a 1 cm UV grade cell and excited in the 267 nm laser beam. As the reaction progressed, the UV/Vis absorption spectrum of the photolyzed sample was measured by using a Perkin–Elmer Lambda 19 UV/Vis spectrometer.

Fs-transient absorption (fs-TA) experiments: The fs-TA measurements were performed based on a commercial femtosecond Ti/sapphire regenerative amplifier laser system. Details of the TA experimental setup are described in ref. [11b]. For the present experiments, the sample solution was excited by a 267 nm pump beam (the third harmonic of 800 nm the regenerative amplifier fundamental) and probed by a white light continue laser beam produced from a rotating CaF_2 plate pumped by the fundamental laser pulses (800 nm). The pump and probe laser beam spot sizes at the sample were about 200 and 100 μm, respectively. The signals were focused into a monochromator and detected by a liquid-N_2 cooled CCD. The time delay between the pump and probe pulse was controlled by an optical delay line and the time resolution of the measurement was ~200 fs. The TA experiments were done for BDP in neat MeCN and 75% H_2O/25% MeCN with a sample concentration of ~1 mM.

Ns-time-resolved resonance Raman (ns-TR^3) experiments: The ns-TR^3 spectra presented here were obtained by using the experimental apparatus and methods described previously.[23,24] Briefly, the sample solution was pump by a 267 nm excitation wavelength provided by the fourth harmonic of a Nd/YAG laser and probed by a 532 nm wavelength provided by the second harmonic of a second Nd/YAG laser. The time delay between the pump and probe laser beams was controlled electronically by a pulse generator and the time resolution of these experiments was ~10 ns. The pump and probe laser beams were lightly focused onto a flowing liquid sample and the Raman scattering was collected via a backscattering configuration and detected by a liquid N_2 cooled CCD. The wavenumber shifts of the resonance Raman spectra were calibrated using the known MeCN solvent Raman bands and the spectra presented were obtained from subtracting of an appropriately scaled probe-before-pump spectrum from the corresponding pump-probe spectrum. The ns-TR^3 measurements were also done for BDP in 75% H_2O/25% MeCN. Normal resonance Raman (RR) experiments using 267 nm excitation were performed for BDP in neat MeCN and 75% H_2O/25% MeCN. The

RR experimental setup is similar to that of the ns-TR[3] but with the probe beam from the second laser blocked. Sample concentrations for the Raman experiments were in the ~1–2 mM range.

Density functional theoretical (DFT) calculations: The DFT calculations reported here were done employing the Gaussian 98 program suite.[55] Complete calculations were done to obtain the geometry optimization, frequencies, and Raman activities of the vibrational modes analytically by using the (U)B3LYP method with a 6-311G** basis set. For the calculations considering the inter-solute-solvent H-bonding interaction, the H-bonded complexes containing the benzoinyl molecule of interest and one or two water molecule(s) H-bonded with the carbonyl oxygen of the molecule were computed for the full geometric optimization, energy and frequency calculations. The H-bonding stabilization energy was estimated based on the energies (including the zero point energy, ZPE) calculated for dissociation of the complex into the free water molecule(s) and the benzoinyl molecule.

Acknowledgements

This research was done in the Ultrafast Laser Facility at the University of Hong Kong and supported by grants from the Research Grants Council of Hong Kong (HKU/7108/02P) and (HKU 1/01C) to D.L.P. W.M.K. thanks the University of Hong Kong for the award of a Research Assistant Professorship.

[1] R. S. Givens, L. W. Kueper, *Chem. Rev.* **1993**, *93*, 55–66.
[2] a) Y. V. Il′ichev, M. A. Schworer, J. Wirz, *J. Am. Chem. Soc.* **2004**, *126*, 4581–4595; b) C. S. Rajesh, R. S. Givens, J. Wirz, *J. Am. Chem. Soc.* **2000**, *122*, 611–618; c) M. A. Hangarter, A. Hormann, Y. Kamdzhilov, J. Wirz, *Photochem. Photobiol. Sci.* **2003**, *2*, 524–535.
[3] a) K. Lee, D. E. Falvey, *J. Am. Chem. Soc.* **2000**, *122*, 9361–9366; b) A. Banerjee, K. Lee, Q. Yu, A. G. Fan, D. E. Falvey, *Tetrahedron lett.* **1998**, *39*, 4635–4638; c) A. Banerjee, D. E. Falvey, *J. Org. Chem.* **1997**, *62*, 6245–6251.
[4] S. Namiki, T. Arai, K. Rujimori, *J. Am. Chem. Soc.* **1997**, *119*, 3840–3841.
[5] H. Sugi, H. Iwamoto, T. Akimoto, H. Ushitani, *Proc. Natl. Acad. Sci. USA* **1998**, *95*, 2273–2278.
[6] M. Lukeman, J. C. Scaiano, *J. Am. Chem. Soc.* **2005**, *127*, 7698–7699.
[7] a) D. Geissler, Y. N. Antonenko, R. Schmidt, S. Keller, O. O. Krylova, B. Wiesner, J. Bendig, P. Pohl, V. Hagen, *Angew. Chem.* **2005**, *117*, 1219–1223; *Angew. Chem. Int. Ed.* **2005**, *44*, 1195–1198; b) R. Schmidt, D. Geissler, V. Hagen, J. Bendig, *J. Phys. Chem. A* **2005**, *109*, 5000–5004; c) T. Eckardt, V. Hagen, B. Schade, R. Schmidt, C. Schweitzer, *J. Org. Chem.* **2002**, *67*, 703–710; d) B. Schade, V. Hagen, R. Schmidt, R. Herbrich, E. Krause, T. Eckardt, J. Bendig, *J. Org. Chem.* **1999**, *64*, 9109–9117.
[8] Y. Zhu, C. M. Pavlos, J. P. Toscanto, T. M. Dore, *J. Am. Chem. Soc.* **2006**, *128*, 4267–4276.
[9] M. Zabadal, A. P. Pelliccioli, P. Klan, J. Wirz, *J. Phys. Chem. A* **2001**, *105*, 10329–10333.
[10] R. S. Givens, P. S. Athey, B. Matuszewski, L. W. Kueper, J. Y. Xue, T. Fister, *J. Am. Chem. Soc.* **1993**, *115*, 6001–6012.
[11] a) C. Ma, W. M. Kwok, W. S. Chan, P. Zuo, J. T. W. Kan, P. H. Toy, D. L. Phillips, *J. Am. Chem. Soc.* **2005**, *127*, 1463–1472; b) C. Ma, W. M. Kwok, W. S. Chan, Y. Du, J. T. W. Kan, P. H. Toy, D. L. Phillips, *J. Am. Chem. Soc.* **2006**, *128*, 2558–2570.
[12] a) R. S. Givens, J. F. Weber, P. G. Conrad, G. Orosz, S. L. Donahue, S. A. Thayer, *J. Am. Chem. Soc.* **2000**, *122*, 2687–2697; b) P. G. Conrad, R. S. Givens, J. F. Weber, K. Kandler, *Org. Lett.* **2000**, *2*, 1545–1547; c) C. Park, R. S. Givens, *J. Am. Chem. Soc.* **1997**, *119*, 2453–2463; d) R. S. Givens, A. Jung, C. Park, J. Weber, W. Bartlett, *J. Am. Chem. Soc.* **1997**, *119*, 8369–8370; e) R. S. Givens, C. Park, *Tetrahedron Lett.* **1996**, *37*, 6259–6262.
[13] a) K. Zhang, J. E. T. Corrie, V. R. N. Munasinghe, P. Wan, *J. Am. Chem. Soc.* **1999**, *121*, 5625–5632; b) M. Fischer, P. Wan, *J. Am. Chem. Soc.* **1999**, *121*, 4555–4562.
[14] A. Specht, S. Loudwig, L. Peng, M. Goeldner, *Tetrahedron Lett.* **2002**, *43*, 8947–8950.
[15] a) C. S. Rajesh, R. S. Givens, J. Wirz, *J. Am. Chem. Soc.* **2000**, *122*, 611–618; b) R. S. Givens, B. Matuszewski, *J. Am. Chem. Soc.* **1984**, *106*, 6860–6861; c) R. S. Givens, P. S. Athey, L. W. Kueper, B. Matuszewski, J. Y. Xue, *J. Am. Chem. Soc.* **1992**, *114*, 8708–8710.
[16] J. M. Peach, A. J. Pratt, J. S. Snaith, *Tetrahedron* **1995**, *51*, 10013–10024.
[17] Y. Shi, J. E. T. Corrie, P. Wan, *J. Org. Chem.* **1997**, *62*, 8278–8279.
[18] a) R. S. Rock, S. I. Chan, *J. Am. Chem. Soc.* **1998**, *120*, 10766–10767; b) R. S. Rock, S. I. Chan, *J. Org. Chem.* **1996**, *61*, 1526–1529.
[19] a) J. C. Sheehan, R. M. Wilson, A. W. Oxford, *J. Am. Chem. Soc.* **1971**, *93*, 7222–7228; b) J. C. Sheehan, R. M. Wilson, *J. Am. Chem. Soc.* **1964**, *86*, 5277–5281.
[20] a) M. C. Pirrung, S. W. Shuey, *J. Org. Chem.* **1994**, *59*, 3890–3897; b) M. C. Pirrung, C. Y. Huang, *Tetrahedron Lett.* **1995**, *36*, 5883–5884; c) M. C. Pirrung, J. C. Bradley, *J. Org. Chem.* **1995**, *60*, 1116–1117; d) M. C. Pirrung, C. Bradley, *J. Org. Chem.* **1995**, *60*, 6270–6276.
[21] J. F. Cameron, C. G. Wilson, J. M. J. Frechet, *J. Am. Chem. Soc.* **1996**, *118*, 12925–12937.
[22] W. S. Chan, C. Ma, W. M. Kwok, P. Zuo, D. L. Phillips, *J. Phys. Chem. A* **2004**, *108*, 4047–4058.
[23] a) W. S. Chan, C. Ma, W. M. Kwok, D. L. Phillips, *J. Phys. Chem. A* **2005**, *109*, 3454–3469; b) P. Zuo, C. Ma, W. M. Kwok, W. S. Chan, D. L. Phillips, *J. Org. Chem.* **2005**. *70*, 8661–8675.
[24] a) C. Ma, P. Zuo, W. M. Kwok, W. S. Chan, J. T. W. Kan, P. H. Toy, D. L. Phillips, *J. Org. Chem.* **2004**, *69*, 6641–6647; b) C. Ma, W. S. Chan, W. M. Kwok, P. Zuo, D. L. Phillips, *J. Phys. Chem. A* **2004**, *108*, 9264–9276.
[25] S. Dym, R. M. Hochstrasser, *J. Chem. Phys.* **1969**, *51*, 2458–2468.
[26] a) D. R. Kearns, W. A. Case, *J. Am. Chem. Soc.* **1966**, *88*, 5087–5097; b) W. A. Case, D. R. Kearns, *J. Chem. Phys.* **1970**, *52*, 2175–2191.
[27] M. B. Ledger, G. Porter, *Trans. Faraday Soc.* **1972**, *68*, 539–553.
[28] H. Lutz, E. Breheret, L. Lindqvist, *J. Phys. Chem.* **1973**, *77*, 1758–1762.
[29] P. M. Rentzepis, *Science* **1970**, *169*, 239–247.
[30] P. J. Wagner, A. E. Kemppaninen, H. N. Schott, *J. Am. Chem. Soc.* **1973**, *95*, 5604–5614.
[31] N. Ohmori, T. Suzuki, M. Ito, *J. Phys. Chem.* **1988**, *92*, 1086–1093.
[32] S.-H. Lee, K.-C. Tang, I.-C. Chen, M. Schmitt, J. P. Shaffer, T. Schultz, J. G. Underwood, M. Z. Zgierski, A. Stolow, *J. Phys. Chem. A* **2002**, *106*, 8979–8991.
[33] B. K. Shah, M. A. J. Rodgers, D. C. Neckers, *J. Phys. Chem. A* **2004**, *108*, 6087–6089.
[34] S. T. Park, J. S. Feenstra, A. H. Zewail, *J. Chem. Phys.* **2006**, *124*, 174707.
[35] J. A. Warren, E. R. Bernstein, *J. Chem. Phys.* **1986**, *85*, 2365–2367.
[36] a) H. E. Zimmerman, *J. Phys. Chem. A* **1998**, *102*, 5616–5621; b) H. E. Zimmerman, *J. Am. Chem. Soc.* **1995**, *117*, 8988–8991.
[37] a) J. A. Pincock, *Acc. Chem. Res.* **1997**, *30*, 43–49; b) J. W. Hilborn, E. MacKnight, J. A. Pincock, P. J. Wedge, *J. Am. Chem. Soc.* **1994**, *116*, 3337–3346.
[38] M. Lipson, A. A. Deniz, K. S. Peters, *J. Am. Chem. Soc.* **1996**, *118*, 2992–2997.
[39] J. Catalan, E. Ferbero, F. Amat-Guerri, *J. Phys. Chem.* **1992**, *96*, 2005–2016.
[40] R. G. Zepp, M. M. Gumz, W. L. Miller, H. Gao, *J. Phys. Chem. A* **1998**, *102*, 5716–5723.
[41] P. K. Das, M. V. Encinas, J. C. Scaiano, *J. Am. Chem. Soc.* **1981**, *103*, 4154–4162.
[42] P. F. McGarry, S. Jockusch, Y. Fujiwara, N. A. Kaprinidis, N. J. Turro, *J. Phys. Chem. A* **1997**, *101*, 764–767.
[43] J. C. Scaiano, *J. Am. Chem. Soc.* **1980**, *102*, 7747–7753.

[44] C. Chudoba, E. T. Nibbering, T. Elsaesser, *J. Phys. Chem. A* **1999**, *103*, 5625–5628.
[45] M. Berger, E. McAlpine, C. Steel, *J. Am. Chem. Soc.* **1978**, *100*, 5147–5151.
[46] C. Reichardt, *Solvent and solvent Effect in Organic Chemistry*, VCH, Weinheim, **1988**.
[47] a) J. H. Horner, E. Taxil, M. Newcomb, *J. Am. Chem. Soc.* **2002**, *124*, 5402–5410; b) M. Newcomb, J. H. Horner, P. O. Whitted, D. Crich, X. Huang, Q. Yao, H. Zipse, *J. Am. Chem. Soc.* **1999**, *121*, 10685–10694.
[48] B. Schade, V. Hagen, R. Schmidt, R. Herbrich, E. Krause, T. Eckardt, J. Bendig, *J. Org. Chem.* **1999**, *64*, 9109–9117.
[49] F. L. Cozens, M. O'Neill, R. Bogdanova, N. Schepp, *J. Am. Chem. Soc.* **1997**, *119*, 10652–10659.
[50] C. P. Andrieux, J. Saveant, A. Tallec, R. Tardivel, C. Tardy, *J. Am. Chem. Soc.* **1996**, *118*, 9788–9789.
[51] a) M. L. Andersen, N. Mathivanan, D. M. Wayner, *J. Am. Chem. Soc.* **1996**, *118*, 4871–4879; b) M. L. Andersen, W. Long, D. M. Wayner, *J. Am. Chem. Soc.* **1997**, *119*, 6590–6595; c) N. Mathivanan, L. J. Johnston, D. M. Wayner, *J. Phys. Chem.* **1995**, *99*, 8190–8195.
[52] R. S. Givens, B. Matuszewski, P. S. Athey, M. R. Stoner, *J. Am. Chem. Soc.* **1990**, *112*, 6016–6021.
[53] J. P. Richard, T. L. Amyes, L. Bei, V. Stubblefield, *J. Am. Chem. Soc.* **1990**, *112*, 9513–9519.
[54] Y. Chiang, A. J. Kresge, P. Salomaa, C. I. Young, *J. Am. Chem. Soc.* **1974**, *96*, 4494–4499.
[55] Gaussian 98, Revision A.11.3, M. J. Frisch, G. W. Trucks, H. B. Schlegel, G. E. Scuseria, M. A. Robb, J. R. Cheeseman, V. G. Zakrzewski, J. A. Montgomery, Jr., R. E. Stratmann, J. C. Burant, S. Dapprich, J. M. Millam, A. D. Daniels, K. N. Kudin, M. C. Strain, O. Farkas, J. Tomasi, V. Barone, M. Cossi, R. Cammi, B. Mennucci, C. Pomelli, C. Adamo, S. Clifford, J. Ochterski, G. A. Petersson, P. Y. Ayala, Q. Cui, K. Morokuma, N. Rega, P. Salvador, J. J. Dannenberg, D. K. Malick, A. D. Rabuck, K. Raghavachari, J. B. Foresman, J. Cioslowski, J. V. Ortiz, A. G. Baboul, B. B. Stefanov, G. Liu, A. Liashenko, P. Piskorz, I. Komaromi, R. Gomperts, R. L. Martin, D. J. Fox, T. Keith, M. A. Al-Laham, C. Y. Peng, A. Nanayakkara, M. Challacombe, P. M. W. Gill, B. Johnson, W. Chen, M. W. Wong, J. L. Andres, C. Gonzalez, M. Head-Gordon, E. S. Replogle, J. A. Pople, Gaussian, Inc., Pittsburgh PA, **2002**.

Received: June 23, 2006
Published online: December 11, 2006

